Journal of Power Sources 275 (2015) 111–125

Contents lists available at ScienceDirect

Journal of Power Sources

journal homepage: www.elsevier.com/locate/jpowsour

# Feasibility study of solid oxide fuel cell engines integrated with sprinter gas turbines: Modeling, design and control

Zhenzhong Jia [a, *], Jing Sun [a], Herb Dobbs [b], Joel King [b]

[a] Department of Naval Architecture and Marine Engineering (NAME), The University of Michigan, Ann Arbor, MI 48109, United States
[b] US Army TARDEC, Non-primary Power Systems Team, Warren, MI 48397-5000, United States

ARTICLE INFO

*Article history:*
Received 5 May 2014
Received in revised form
28 October 2014
Accepted 31 October 2014
Available online 1 November 2014

*Keywords:*
Solid oxide fuel cell (SOFC)
Gas turbine (GT)
Load following
Design
Control analysis

ABSTRACT

Conventional recuperating solid oxide fuel cell (SOFC)/gas turbine (GT) system suffers from its poor dynamic capability and load following performance. To meet the fast, safe and efficient load following requirements for mobile applications, a sprinter SOFC/GT system concept is proposed in this paper. In the proposed system, an SOFC stack operating at fairly constant temperature provides the baseline power with high efficiency while the fast dynamic capability of the GT-generator is fully explored for fast dynamic load following. System design and control studies have been conducted by using an SOFC/GT system model consisting of experimentally-verified component models. In particular, through analysis of the steady-state simulation results, an SOFC operation strategy is proposed to maintain fairly constant SOFC power (less than 2% power variation) and temperature (less than 2 K temperature variation) over the entire load range. A system design procedure well-suited to the proposed system has also been developed to help determining component sizes and the reference steady-state operation line. In addition, control analysis has been studied for both steady-state and transient operations. Simulation results suggest that the proposed system holds the promise to achieve fast and safe transient operations by taking full advantage of the fast dynamics of the GT-generator.



## 1. Introduction

The hybrid solid oxide fuel cell/gas turbine (SOFC/GT) system has the potential to achieve ultra-high efficiency, ultra-low emissions, and fuel flexibility. By leveraging the complementary features of these two power sources, the integrated system could achieve up to 65% fuel-to-electric efficiency for stationary applications [1–5]. For mobile applications, the SOFC/GT system has also been considered for auxiliary power units (APUs) for ground vehicles [6,7], and aircrafts [8], the primary electric propulsion system for mid-sized vehicles [9], and marine power generations [10,11]. While the SOFC/GT concept is very appealing for mobile applications from the efficiency perspective, its feasibility depends critically on the dynamic characteristics. In particular, since load following is one of the most essential requirements for mobile applications, the SOFC/GT system must be able to make fast load transients without causing negative impact on the components and system life span [7,12].

Many studies have shown that the SOFC/GT system has very limited dynamic capability due to system characteristics and stringent operation requirements [7,13]. First, the large thermal capacitance of the SOFC and the slow fuel path dynamics often lead to slow transient response. Typical power transients might take several minutes or longer while the thermal transients might take hours to settle [14]. Second, fast changes in the SOFC operation are often prohibited in order to prevent possible damages caused by thermally induced stresses. In particular, the cell temperature needs to be kept fairly constant for high efficiency and long life cycle operation [14]. Third, the closed thermal and mechanical couplings, which are essential for high efficiency operation, make fast and safe load following extremely challenging [7]. Hence, effective strategies that can extend the dynamic capabilities of the SOFC/GT system for improved load following performance are becoming critical enablers for its widespread application to mobile platforms [7].

### 1.1. Conventional recuperating-SOFC/GT systems

Most papers in the literature [5] focus on the design [14,21] and optimization [22] of the recuperating-SOFC/GT (referred to as R-

* Corresponding author.
*E-mail addresses:* zhenzjia@umich.edu (Z. Jia), jingsun@umich.edu (J. Sun).

http://dx.doi.org/10.1016/j.jpowsour.2014.10.203
0378-7753/

**Nomenclature**

| | |
|---|---|
| APU | auxiliary power unit |
| CB | catalytic burner |
| ERD | energy recovery device |
| GT | gas turbine |
| G/M | generator/motor |
| HEX | heat exchanger |
| MPC | model-based predictive control |
| R-SOFC/GT | recuperating-SOFC/GT |
| SOFC | solid oxide fuel cell |
| S-SOFC/GT | sprinter-SOFC/GT |
| $AR$ | SOFC excess air ratio [-] |
| $ER$ | turbine expansion ratio [-] |
| $FU$ | SOFC fuel utilization ratio [-] |
| $I_{com}$ | current density command [$A\cdot m^{-2}$] |
| $J$ | turbocharger inertia [$kg\cdot m^2$ ] |
| $K_p$ | compressor surge margin [-] |
| $N$ | turbo-shaft speed [RPM ] |
| $\tilde{N}$ | normalized shaft speed [-] |
| $N_{c\_design}$ | designed compressor shaft speed [RPM] |
| $N_{cell}$ | number of SOFC cells [-] |
| $N_{des}$ | desired shaft speed [RPM] |
| $N_{tc}$ | corrected turbine speed [$RPM\cdot K^{-0.5}$] |
| $\tilde{N}_{tc}$ | normalized turbine speed [-] |
| $N_{t\_design}$ | designed turbine shaft speed [RPM] |
| $PR$ | compressor pressure ratio [-] |
| $P_{base}$ | baseline power demand [W] |
| $P_c$ | compressor consumed power [W] |
| $P_{gen}$ | generator load [W] |
| $P_{peak}$ | peak power demand [W] |
| $P_t$ | turbine generated power [W] |
| $P_{sofc}$ | SOFC power [W] |
| $T_{air}$ | SOFC inlet air temperature [K] |
| $T_{cb}$ | burner temperature [K] |
| $T_{sofc}$ | SOFC cell temperature [$K$] |
| $T_{t1\_design}$ | designed turbine inlet temperature [K] |
| $\tilde{W}$ | normalized compressor mass flow [-] |
| $W_{air}$ | SOFC inlet air mass flow rate [$kg\cdot sec^{-1}$] |
| $W_c$ | compressor mass flow [$kg\cdot sec^{-1}$] |
| $W_{c\_design}$ | designed compressor mass flow [$kg\cdot sec^{-1}$] |
| $W_f$ | mass flow rate of the fuel supply [$kg\cdot sec^{-1}$] |
| $\eta_{comp}$ | compressor isentropic efficiency [-] |
| $\eta_m$ | turbine mechanical efficiency [-] |
| $\eta_{net}$ | total system efficiency [-] |
| $\eta_{turb}$ | turbine isentropic efficiency [-] |
| $\phi_{choke}$ | corrected turbine swallowing capacity [$kg\cdot K^{0.5}\cdot sec^{-1}\cdot bar^{-1}$] |
| $\phi_{norm}$ | normalized turbine flow [-] |
| $\phi_t$ | corrected turbine flow [$kg\cdot K^{0.5}\cdot sec^{-1}\cdot bar^{-1}$] |

SOFC/GT in this paper) systems, in which a recuperating GT, whose primary function is to recuperate the exhaust energy, is integrated with the SOFC. Fig. 1 presents a typical design procedure for the conventional R-SOFC/GT system. First, the SOFC design point can be determined according to the rated power demand, SOFC data, and empirical parameters such as the fuel utilization (FU) and power split ratio. Second, the compressor-turbine design point can be determined by matching the pressure, temperature, and mass flow requirements identified in the first step. Third, the heat exchanger (HEX) parameters are determined and the design point and the part-load (i.e., off-design) performance are evaluated. The design process is iterated if necessary. Computer programs, which could automate the design process, have also been developed to optimize the overall system performance [22].

In parallel to the design and optimization of the SOFC/GT system, the control and system integration solutions, especially those aimed at addressing dynamic operations, have also been explored [12,14]. In Refs. [14], a multi-loop feedback control scheme has been

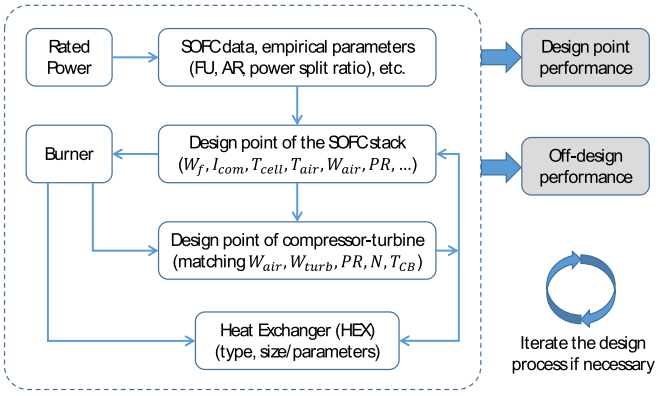


**Fig. 1.** A representative design procedure for conventional recuperating-SOFC/GT systems.

developed by controlling the current, fuel supply, and air flow (by manipulating the generator load) for safe part-load operations. In Refs. [15], an incremental step reference governor (IS-RG) has been developed for fast load step-up transition while avoiding potential system shut-down. In Refs. [12], a model-based predictive control (MPC) strategy, which could handle various operational constraints, has been developed for coordinated power and thermal management. In addition to finding effective control strategies without modifying the existing system setup, alternative solutions that augment the SOFC/GT system with new features/functionalities have also been investigated. In Refs. [16], the variable geometry turbine (VGT) technique has been used to address the shut-down problem and improve the transient performance during abrupt load changes. Similar techniques, e.g., the variable geometry compressor (VGC), have also been used to improve the part-load performance [17]. By taking full advantage of the bi-directional operation of the generator/motor (G/M), we showed that improved load following and thermal management can be achieved, power and energy requirements for the battery (which provides the bridging power for step-up transients and absorbs the excessive power for step-down transients) can be reduced, and overall system performance can be enhanced [7].

However, one common problem of the conventional R-SOFC/GT systems is that their transient performance (e.g., load following, thermal transients) is dominated by the transient limitations of the SOFC (the primary power source of the R-SOFC/GT system). The GT (the component with fast dynamics) is mainly used as an energy recovery device (ERD) to recuperate the otherwise wasted exhaust energy for air delivery (the primary task) while limited remaining shaft power can be used to drive the generator to produce additional electric power (often less than 20% of the total power). Moreover, the electric power generation capability of the GT-generator assembly is limited by its size, which is often optimized to match the SOFC in the R-SOFC/GT systems [17]. Therefore, one cannot take advantage of the fast shaft dynamics of the GT-

**Table 1**
Recuperating-SOFC/GT system versus sprinter-SOFC/GT system.

| Systems | Conventional R-SOFC/GT system | Proposed S-SOFC/GT system |
|---|---|---|
| SOFC | - Primary power source ($P_{sofc} \approx 80\% P_{net}$)<br>- Varying SOFC power/temperature over the entire load region<br>- Fairly const. FU (FU = 75–90%) | - "Down-sized" to provide the baseline power<br>- Fairly constant SOFC power/temperature<br>- Substantial FU variation (e.g., ~90% → ~50% from baseline to peak power) |
| GT-generator | - Energy recuperation (GT), auxiliary device (generator)<br>- Limited power generation capability<br>- $P_{gen}/P_{sofc} \approx 1/4$ | - Important power generation device<br>- Significantly enhanced power generation capability for the GT-generator<br>- $P_{gen}/P_{sofc}$ can vary from 20% to 80+% |
| Load following | - Both SOFC and GT-generator are used<br>- Limited by SOFC slow dynamics<br>- Fast dynamics of GT-generator could not be used due to its limited size | - Fast dynamic load following by taking advantage of GT-generator fast dynamic capability<br>- SOFC (provides constant baseline power) |

generator assembly for improved transient operations in conventional R-SOFC/GT systems. In addition, the strong thermal and mechanical couplings [7] and the lack of independent air control [14] further complicate the system operation.

### 1.2. Sprinter-SOFC/GT system: concept and research problems

To meet the safe, efficient and fast load following requirements for mobile applications [7], a new sprinter-SOFC/GT (referred to as S-SOFC/GT in this paper) system concept (see Table 1) will be pursued in this study. In the proposed S-SOFC/GT system, a "down-sized" SOFC stack, which is operated at fairly constant temperature, is integrated with a sprinter GT-generator assembly. This sprinter GT-generator could produce a considerable amount of power very quickly through top speed operation to meet the desired high power demand for a brief period. In the proposed system, only the fast dynamic component, i.e., the GT-generator, will be used for dynamic load following, while the constant-loading SOFC is mainly used to provide the baseline power with high efficiency. Compared with the conventional R-SOFC/GT system, in which both the SOFC and GT-generator are used for load following, the proposed S-SOFC/GT system has the potential to achieve: (a) fast load following by taking full advantage of the fast dynamic capability of the GT-generator assembly; (b) efficient and long life cycle operation by running the SOFC at fairly constant cell temperature.

To the authors' best knowledge, the S-SOFC/GT concept proposed herein has not been explored in the literature. The system design, dynamic operation and controls associated with the S-SOFC/GT system need to be investigated, given the differences (see Table 1) between the R-SOFC/GT system and the proposed S-SOFC/GT system. The design procedure (Fig. 1) for the conventional R-SOFC/GT system is not suited for the proposed S-SOFC/GT system for several reasons. First, the design process from the full-load design point (for the nominal power) to the part-load off-design analysis does not apply to the S-SOFC/GT system because there are at least two operation points (i.e., the baseline load and the peak load points) to be determined. Second, maintaining fairly constant SOFC power/temperature for all load conditions in the S-SOFC/GT system is a main design requirement which may not be possible in the R-SOFC/GT systems because load following requires varying SOFC power in a wide range in the recuperating systems. Third, design guidelines for recuperating systems, e.g., typical parameter values for the fuel utilization ($FU \approx 0.85$) and power split ratio ($P_{gen}$:$P_{sofc} \approx 1$:4), cannot be directly applied to the proposed system since their values will vary significantly (see Table 1 and Section 3.3) over the entire operation envelopes. Fourth, the proposed system has significantly extended operation regions for the sprinter GT-generator (e.g., air/gas mass flows, pressures, temperatures and generator power). Therefore, new system design procedure/methodology suited for the proposed S-SOFC/GT systems needs to be developed.

The proposed system also has different control implications. For example, both the load following and air flow are managed through the generator power, which poses a more serious challenge for the transient operations in the proposed system since the air flow and generator power will vary significantly over the entire operation envelope (see Section 3.3). Hence, control and system integration solutions, which could tackle the closed thermal/mechanical couplings in the system, need to be explored. The ultimate goal of this research is to establish a new SOFC/GT design framework to meet the high efficiency and long life span requirements for future mobile power applications. For this particular paper, we mainly focus on the system modeling and design, as well as the feasibility problem, i.e., whether the proposed S-SOFC/GT system has the ability to achieve the desired objectives of: (a) keeping fairly constant SOFC power and temperature over the entire load region; (b) achieving fast and safe load following. The control algorithms will be developed for coordinated power and thermal management in the future.

The remainder of this paper is organized as follows: Section 2 presents the system operation principle and the modeling of key system components. Section 3 presents an operational strategy to maintain fairly constant SOFC power and temperature over the entire load region and elucidates a design procedure for the proposed S-SOFC/GT system. The steady-state performance of the designed S-SOFC/GT system is also discussed in this section. Section 4 presents the control analysis for steady-state operations and the feasibility study of transient operations. Finally, the summary and future work are given in Section 5.

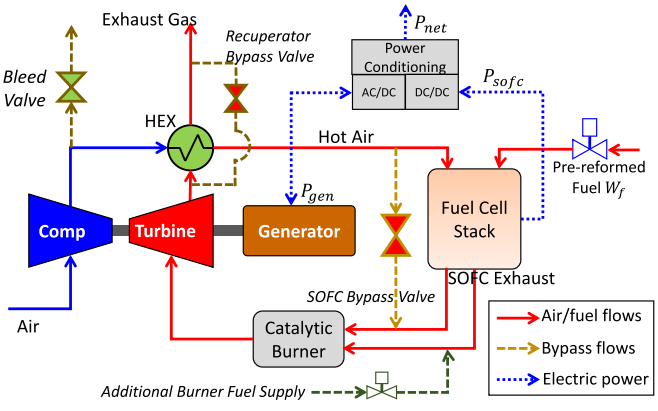


**Fig. 2.** The integrated SOFC/GT system configuration.

## 2. System modeling and operation principles

### 2.1. System configuration and operation principles

Fig. 2 presents the integrated SOFC/GT system configuration. The key system components include an SOFC stack, a catalytic burner (CB), a compressor, a turbine, a generator, and a heat exchanger (HEX). The air is supplied to the cathode side of the SOFC, while pre-reformed fuel is fed to the anode side. The SOFC exhaust can be fed into the burner where the unused fuel is burned to increase the flow temperature, which will be used to drive the turbine. This provides a mechanism to recuperate the exhaust energy for improved system efficiency. The turbine drives both the compressor (delivers air to the fuel cell stack) and the generator (produces additional electric power) through a mechanical shaft. The turbine exhaust can be fed into the HEX to pre-heat the air delivered to the SOFC [7].

Note that the recuperating and sprinter SOFC/GT systems have the same base components and configuration. The main differences are: (a) the relative size of the GT-generator with respect to the SOFC; and (b) the operation principles. In particular, the S-SOFC/GT system has a larger relative size ratio of the GT-generator with respect to the SOFC than its recuperating counterpart since more power is produced by the GT-generator in the sprinter system.

The system setup (w/o valves) presented in Fig. 2 is the most common configuration (referred to as the basic configuration in this paper) for SOFC/GT systems [17]. It should be noted that there are also many variant setups, e.g., the SOFC/GT system with a dual-spool GT [4] and multiple HEXs. Moreover, the basic system setup can be augmented with additional features/functionalities, e.g., variable geometry compressor/turbine (VGC/VGT) [17], bypass valves [4], G/M dual mode operation and energy storage [7]. In particular, there might be a mismatch between the SOFC air flow demands and that supplied by the compressor, leading to over-cooling or over-heating of the SOFC during operations. In this case, bypass valves [18] or a heater/cooler [19] are often used to increase the operating range at the expense of system efficiency [17] and complexity. For example, in the Siemens–Westinghouse test facility, an SOFC bypass valve and a recuperator bypass valve (Fig. 2) have been used to control the inlet air flow rate and temperature, respectively [4]. Similar valves have also been used in the Department of Energy *Hyper* (Hybrid Performance Project) hardware-in-the-loop (HIL) simulation facility [20]. In this paper, we mainly focus on the design and control problems for the basic system setup while the problems associated with the augmented system setups will be investigated in future studies.

### 2.2. System modeling

There are very few SOFC/GT experimental facilities successfully installed in the world. Siemens–Westinghouse demonstrated a 220 kWe system at the University of California, Irvine (UC-Irvine) [3] and a 300 kWe system at Pittsburgh [31]. The Mitsubishi Heavy Industries, Ltd. (MHI, Japan) tested a 75 kWe SOFC-MGT facility and a 200 kWe class system [32]. The National Energy Technology Laboratory (NETL) also constructed the *Hyper* facility [20], which combines an SOFC-emulating burner and real GT-generator assembly, to support the HIL simulation. Due to the limited availability of SOFC/GT test facilities and the lack of experimental data in the open literature, simulation-based study remains the only viable option for most research groups in the world [5,14]. Detailed reviews of dynamic SOFC models and the SOFC/GT system models can be found in Refs. [5,33].

Given the difficulties in the system-level experimental validations and the importance of model-based analysis, it is critical to use experimentally-verified or experimentally-fitted component models and validate the flow pressure and temperature distributions and the connections between different components. Otherwise, the simulation might generate questionable or even incorrect results. To this end, in this paper, the SOFC model used in Refs. [6,7] has been improved and validated against available experiment data. The other component models, e.g., the compressor and turbine, have been revisited and enhanced, and verified with available experiment data. The modeling work lays the foundation for the subsequent design and control studies. In the sequel, we introduce the SOFC and GT modeling, while the modeling of other components such as the burner [15] and HEX [37] can be found in the references.

#### 2.2.1. Tubular SOFC model

In this study, tubular SOFC cells developed by Siemens are used due to their advantages in thermal expansion and gas sealing [23]. In the tubular design (Fig. 3 (a)), the pre-heated air enters the air-feeding tube (injector) and travels to the closed end. Pre-reformed fuel enters the SOFC outside the tube from the closed end. The air and fuel both flow along the cell in the same direction from the closed end toward the open end; this configuration is known as the co-flow configuration [23]. A first principle based SOFC model has been developed by considering electro–chemical reaction, mass and energy balances [6]. Finite volume discretization (see Fig. 3 (a)) method [23,24] is used. One can refer to [23,24,34] for the modeling details. In addition, the fuel is assumed to be a mixture of six species, consisting of methane ($CH_4$), carbon monoxide (CO), carbon dioxide ($CO_2$), hydrogen ($H_2$), steam ($H_2O$) and nitrogen ($N_2$), where the concentration ratios can be varied to reflect different pre-reforming results.

It should be noted that internal reforming is assumed and issues related to external pre-reforming [14] are not addressed in this work. With external reforming, anode gas recirculation is usually required in order to provide the steam required for reforming, and steam-to-carbon-ratio [14], [40] has to be well controlled. Those issues have been addressed for R-SOFC/GT system (see, e.g., [21]). We expect that they could result in similar additional challenges for the proposed S-SOFC/GT system, and full analysis of their impact is worthy of further research effort.

The dynamic (tubular) SOFC model has been implemented in the Matlab/Simulink environment. The model predicts various temperatures, gas compositions, and all the electrochemical-related variables (cell voltage, current density, power, etc.). The cell (geometric and material-related) parameters are taken from Ref. [23]. Fig. 3 (b) shows the simulated temperature profiles along the axial direction for different temperature layers; the results agree with those in Ref. [23]. In Fig. 4, the simulation results of the cell voltage and power are compared to the actual test data taken from Ref. [1]. Less than 3% error between the model and the test data has been achieved over the entire current density range.

#### 2.2.2. Turbomachinery model

The turbomachinery model incorporates the shaft rotational dynamics, the compressor and the turbine model. Only the shaft dynamics is considered [15], while map-based models (sufficient for the SOFC/GT system [14]) are used for turbine and compressor. The main variables used in those models include pressure $p$, mass flow rate W, temperature $T$ and power $P$, as shown in Fig. 5. Note that the subscripts denote the component ($c$ for compressor and $t$ for turbine) and the inlet and outlet ((1) or (2), respectively).

The turbocharger rotational dynamics [15] is determined by the turbine generated power $P_t$, the power required to drive the compressor $P_c$ and the power drawn by the generator $P_{gen}$ as:

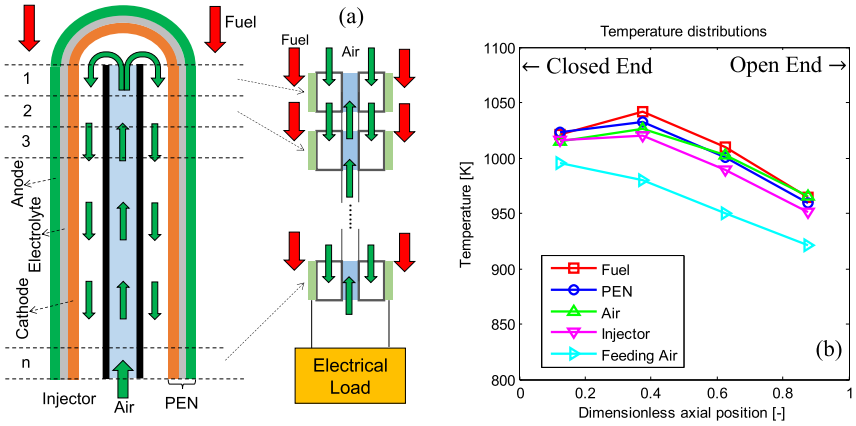


**Fig. 3.** (a) Finite volume discretization. (b) Simulated cell temperature distributions.

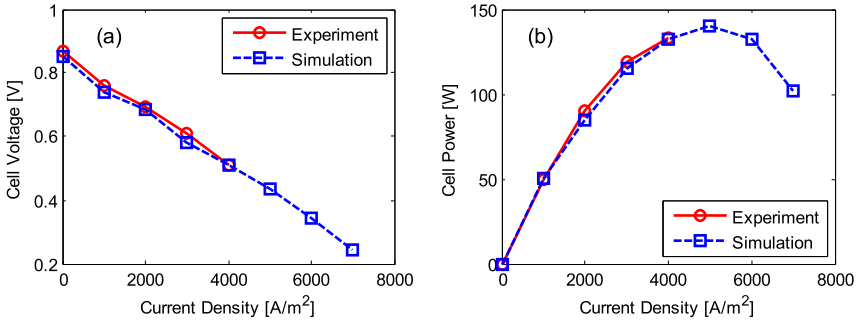


**Fig. 4.** Simulation and experiment results: (a) cell voltage and (b) cell power versus current density.

$$\frac{dN}{dt} = \frac{P_t\eta_m - P_c - P_{gen}}{\alpha \cdot N \cdot J} = \frac{P_{tc} - P_{gen}}{\alpha \cdot N \cdot J}, \tag{1}$$

where $N$ is the turbocharger speed, $J$ is the turbocharger inertia, $\alpha = (2\pi/60)^2$ is a factor used to convert the shaft speed from RPM (round per minute) to $rad \cdot sec^{-1}$ (radian per second), and $\eta_m$ is the turbine mechanical efficiency that accounts for energy losses due to the friction. Instead of using (1), alternative formulas presented in Ref. [35] can also be used to model the speed-dependent bearing loss terms.

The compressor and turbine models provide the thermodynamic equations for the input–output relations of the working fluid based on pressure ratio, shaft speed and temperature (referred to as Type-I models in Ref. [28]). Instead of using look-up table (LUT) [6], it is preferred to use curve fitting methods [28,29] to express the maps in compact functional forms with coefficients determined from experiment data. This guarantees a smooth interpolation and allows reliable extension of the maps beyond the region where experimental data is available [15].

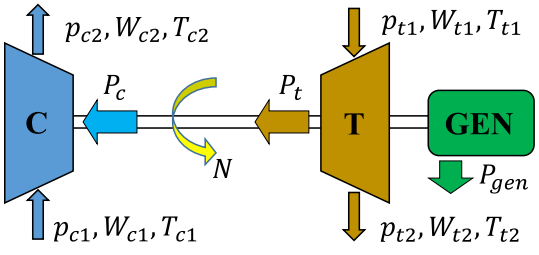


**Fig. 5.** Compressor, turbine, shaft and generator schematic.

Define the normalized mass flow $\tilde{W}$, the normalized shaft speed $\tilde{N}$ and the pressure ratio $PR$ as:

$$\tilde{W} = \frac{W_c}{W_{c\_design}}, \quad \tilde{N} = \frac{N}{N_{c\_design}}, \quad \mathrm{PR} = \frac{p_{c2}}{p_{c1}}, \tag{2}$$

where $W_{c\_design}$ and $N_{c\_design}$ are the air mass flow and shaft speed at the compressor design point. By using the normalized parameters, one can easily apply the similarity principle [25] to scale existing compressor maps to meet specific requirements without changing the already-fitted coefficients. Analogous to the Zero Slope Line Method (ZSLM) in Refs. [28], the flow parameter $\tilde{W}$ can be expressed as a function of pressure ratio $PR$ and the normalized speed $\tilde{N}$. First, the curve connecting the maximum mass flows on each speed line (often referred to as the zero slope line) can be characterized as follows:

$$\begin{cases} \tilde{W}_{top} = f_{Wtop}\left(\tilde{N}\right) = p_2\tilde{N}^2 + p_1\tilde{N} + p_0 \\ PR_{top} = f_{PRtop}\left(\tilde{W}_{top}\right) = c_a\tilde{W}_{top}^{c_b} + c_c \end{cases}, \tag{3}$$

where $PR_{top}$ is the pressure ratio corresponding to $\tilde{W}_{top}$. Then, the speed lines can be modeled as:

$$\frac{\tilde{W}}{\tilde{W}_{top}} = 1 + \alpha_c\left(1 - exp\left(k\left(\frac{PR}{PR_{top}} - 1\right)\right)\right), \ \alpha_c = q_0 \exp\left(q_1\tilde{N}\right), \tag{4}$$

where $k$, $q_0$ and $q_1$ are constant parameters to be determined from the experimental data.

The surge margin $K_p$, defined in (5), should always be kept above 5–10% for safe operation [36].

$$K_p = \frac{PP_{\text{surge}}/W_c(\text{surge})}{PR/W_c}. \tag{5}$$

The compressor efficiency can be fitted as a polynomial function [29] of $\tilde{N}$ and $\tilde{W}$ as:

$$\eta_{comp} = f_{\eta_{comp}}\left(\tilde{N}, \tilde{W}\right) = e_0 + e_1\tilde{N} + e_2\tilde{N}^2 + e_3\tilde{W} + e_4\tilde{W}^2 + e_5\tilde{N}\tilde{W}. \tag{6}$$

Weighted least squares method can be used to determine the coefficients. As shown in Fig. 6 (a), good agreement between the curve fitting results and experiment data has been achieved for the Garrett [30] GTX2867R compressor (used as the reference compressor for S-SOFC/GT system design in Section 3) by using (2)–(4). In addition, the second order polynomial [29] expressed in (6) has been extended to the third order (expression not shown here) for better fitting results of the compressor efficiency, as shown Fig. 6 (b).

For the turbine, define the corrected turbine flow $\phi_t$, the corrected turbine speed $N_{tc}$, the expansion ratio $ER$, the normalized flow $\phi_{norm}$ and the normalized speed $\tilde{N}_{tc}$ as follows:

$$\phi_t = \frac{W_t\sqrt{T_{t1}}}{p_{t1}}, \quad N_{tc} = \frac{N}{\sqrt{T_{t1}}}, \quad ER = \frac{p_{t1}}{p_{t2}}, \tag{7}$$

$$\phi_{\text{norm}} = \frac{\phi_t}{\phi_{\text{choke}}}, \quad \tilde{N}_{tc} = \frac{N_{tc}}{N_{tc\_\text{design}}} = \frac{N}{N_{t\_\text{design}}}\cdot\frac{\sqrt{T_{t1\_\text{design}}}}{\sqrt{T_{t1}}}, \tag{8}$$

where $\phi_{choke}$ is the corrected turbine flow capacity when turbine choking occurs, $N_{t\_\text{design}}$ and $T_{t1\_\text{design}}$ are the turbine speed and turbine inlet temperature at the design point. Fig. 7 presents the normalized mass flow $\phi_{norm}$ and efficiency maps of a typical radial turbine for diesel engine turbochargers [26,27]. However, formulas (based on typical nozzle flow equations) given in Refs. [28], which are often used for turbine modeling, do not give good results. An alternative curve fitting method (see Fig. 7 (a) for fitting results) is proposed as follows. The normalized flow $\phi_{norm}$ can be expressed as a function of the expansion ratio $ER$:

$$\phi_{norm} = 1 - \phi_b \cdot exp(-ER/\phi_c), \tag{9}$$

where the speed-dependent terms $\phi_b$ and $\phi_c$ are determined as:

$$\phi_b = \phi_{b0}\cdot\tilde{N}_{tc}^{\phi_{b1}} + \phi_{b2}, \ \phi_c = \phi_{c0}\tilde{N}_{tc} + \phi_{c1}. \tag{10}$$

The turbine efficiency can often be expressed as a polynomial function [26] of the blade-speed ratio. Fig. 7 (b) presents the fitting result. The standard thermodynamic equations to compute the compressor and turbine outlet temperature and power can be found in Ref. [28]. It should be noted that variation of turbine coefficient values (due to the change of exhaust compositions) can often be neglected [36].

## 3. System design and steady-state performances

The proposed S-SOFC/GT system is intended to be used as the primary electric propulsion system for military ground vehicles. The proposed system could meet the baseline power requirement $P_{base}$ (e.g., $P_{base}$ = 110 kW) when working at recuperation mode. Moreover, by running the GT in boosting mode, the system could meet a much higher power demand $P_{peak}$ (e.g., $P_{peak}$=170 kW) for tactic/battle-filed maneuvers. It should be noted that while the results reported in this paper are specific for this targeted power, the proposed design procedure and analysis methodology are more general, and can be applied to other size power systems.

Recall that one of the most critical requirements for the proposed S-SOFC/GT system is to keep constant SOFC power and temperature overall conditions. In this section, we will investigate the feasibility problem, i.e., whether the power range [$P_{base}$, $P_{peak}$] can be covered while maintaining fairly constant SOFC power and temperature. If this is the case, operating strategies to meet different power demands need to be studied as well. The system design will also help to determine the sizes of different components (e.g., SOFC, GT and HEX) and the steady-state feed-forward operation line for the integrated system, as will be shown in the following sections.

In this paper, system design and operation strategies will be investigated for the basic system setup (see Section 2.1). Section 3.1 elucidates an effective operation strategy to coordinate the system inputs to keep fairly constant (steady-state) SOFC power and

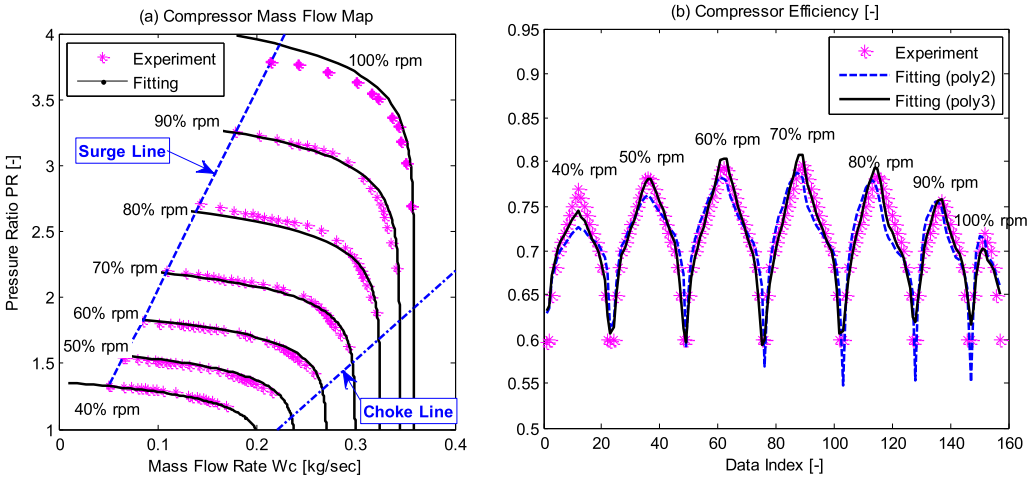


**Fig. 6.** Compressor mass flow and efficiency maps: experimental and curve fitting results. The $x$-axis label 'data index' in figure (b) indicates the index number of experiment data points selected in the compressor map.

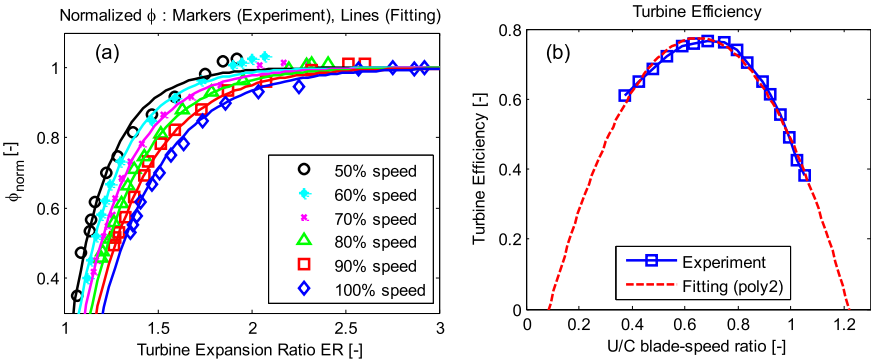


**Fig. 7.** Turbine mass flow and efficiency maps: experimental and curve fitting results.

temperature overall load conditions. In Section 3.2, a design procedure is developed for the proposed S-SOFC/GT system by including the proposed operation strategy. The design procedure will help to determine the component sizes and the steady-state operation line. Section 3.3 shows the steady-state performance of the proposed S-SOFC/GT system. System design and operation strategies associated to the augmented system setups, which are expected to be different from those of the basic system setup, will be investigated in future studies.

### 3.1. An effective operation strategy to maintain constant SOFC power and temperature

The integrated SOFC/GT system has three inputs, namely, the SOFC fuel mass flow rate $W_f$, the SOFC current density command $I_{com}$, and the generator load $P_{gen}$ [15]. In addition to the $W_f$ and $I_{com}$ inputs, there are some other parameters, e.g., the SOFC inlet air mass flow $W_{air}$ and temperature $T_{air}$, which will affect the SOFC performance (SOFC inputs: $W_f$, $I_{com}$, $W_{air}$ and $T_{air}$). Note that the inlet air mass flow $W_{air}$ is often controlled by Ref. $P_{gen}$ [14] while $T_{air}$ is the HEX output which depends on the fuel mass flow $W_f$, air mass flow $W_{air}$, turbine outlet temperature $T_{t2}$, and HEX parameters (e.g., size and material related coefficients).

In the proposed S-SOFC/GT system, a substantial variation of the turbine power is required to meet varying power demands over the entire load region since the SOFC power remains constant at all conditions. In this case, large variations of the turbine mass flow $W_t$ (which equals the sum of fuel mass flow $W_f$ and air mass flow $W_{air}$) and the turbine inlet/outlet temperatures (which will affect the SOFC inlet air temperature $T_{air}$ through the HEX) are expected. All these variations are expected to have significant influence on the SOFC performance given the closed couplings among system components [17]. Hence, it is necessary to perform sensitivity analysis and find effective strategies to coordinate the system inputs to keep fairly constant SOFC power and temperature over the entire load range. To this end, an SOFC stack (with a nominal power around 88 kW when operated at 1040 K) consisting of 960 tubular cells (see Section 2.2) will be used in the following analysis. In addition, a slightly scaled (scaled up by a factor of 1.091) Garrett [30] compressor (see Fig. 6 for the original map) and the radial turbine in Fig. 7 are selected in the following case study. The HEX is sized to keep the SOFC inlet temperature $T_{air}$ within safe range.

To keep fairly constant SOFC power $P_{sofc}$, the current density $I_{com}$ is expected to be relatively constant (i.e., with a very limited variation range) over the entire load range. With a fixed $I_{com}$ input, the main degrees of freedom for operating the hybrid system are fuel mass flow $W_f$ and air flow $W_{air}$ (controlled by Ref. $P_{gen}$). Fig. 8 presents the SOFC performance for constant $I_{com}$ input ($I_{com}$=1950$A\cdot m^{-2}$) and varying $W_{air}$ and $W_f$. Note that $P_{sofc}$ and $U_{sofc}$ (cell voltage) have very similar distributions over the $W_{air}$~$W_f$ plane. This is expected for fixed $I_{com}$ input since $P_{sofc}=U_{sofc}\cdot I_{com}\cdot A_{sofc}$ where $A_{sofc}$ represents the surface area where the electro–chemical reaction takes place. In addition, when we reduce the air flow $W_{air}$ while keeping fuel flow $W_f$ fixed, the parameters $T_{sofc}$, $P_{sofc}$ and $U_{sofc}$ all increase due to the reduced cooling effect, as shown in Fig. 8. The solid lines shown in the figures correspond to a constant SOFC temperature operational condition, where $T_{sofc}$ = 1040 K.

Along the constant temperature line, the key operational variables, including $P_{sofc}$, $U_{sofc}$, and $T_{air}$ (the SOFC inlet air temperature), are plotted in Fig. 9. As shown in Fig. 9 (c), when more air (note that $W_{air}$ increases with respect to $W_f$) is delivered to the SOFC, the SOFC inlet air temperature $T_{air}$ should be increased to counteract the cooling effect, thereby maintaining fairly constant $T_{sofc}$. In addition, as shown in Fig. 9 (b), with a constant cell temperature, the actual cell voltage $U_{sofc}$ increases with respect to the fuel flow $W_f$ due to the increased open circuit voltage $U_{OCV}$ (see the Nernst equation in Ref. [24]). As a result, the SOFC power $P_{sofc}$ increases with respect to $W_f$ when both $T_{sofc}$ and $I_{com}$ are fixed, as shown in Fig. 9 (a). Therefore, in order to keep constant $P_{sofc}$ and $T_{sofc}$ over the entire load range, we need to reduce $I_{com}$ when increasing $W_f$, i.e., $I_{com}$ should be a decreasing function of $W_f$.

Next, with the fixed $I_{com}$ constraint being relaxed, we investigate the relations among system input variables to keep $P_{sofc}$ and $T_{sofc}$ both fairly constant over the entire load range. Fig. 10 (a) shows the iso-surface for constant $P_{sofc}$ ($P_{sofc}$=88.5 kW), the iso-surface for constant $T_{sofc}$ ($T_{sofc}$=1040 K) and the intersection line (the dashed line in the figure) of these two iso-surfaces. In theory, both $P_{sofc}$ and $T_{sofc}$ will be exactly constant along the intersection line. However, as shown in Fig. 10 (b), small variations of $P_{sofc}$ ($P_{sofc}$=88.5±0.5 kW) and $T_{sofc}$ ($T_{sofc}$=1040±2 K) are observed along the intersection line, mainly due to the numerical errors when calculating the iso-surfaces. Nevertheless, we see that fairly constant SOFC power and temperature can be achieved along the intersection line. Fig. 11 presents the relations among the SOFC inputs (i.e., $W_f$, $I_{com}$, $W_{air}$ and $T_{air}$) along the intersection line. It should be pointed out that although these results are generated by using specific GT maps and HEX parameters for this specific case study, the relations in Fig. 11 to maintain constant SOFC power and temperature are very strong and are expected to hold (at least, hold at a qualitative level) for various component (e.g., SOFC and GT) parameters. This has been verified in our simulation studies.

$$W_{air} = f_{Wair}\left(W_f\right) = k_{Wair2}\left(W_f\right)^2 + k_{Wair1}W_f + k_{Wair0}, \qquad (11)$$

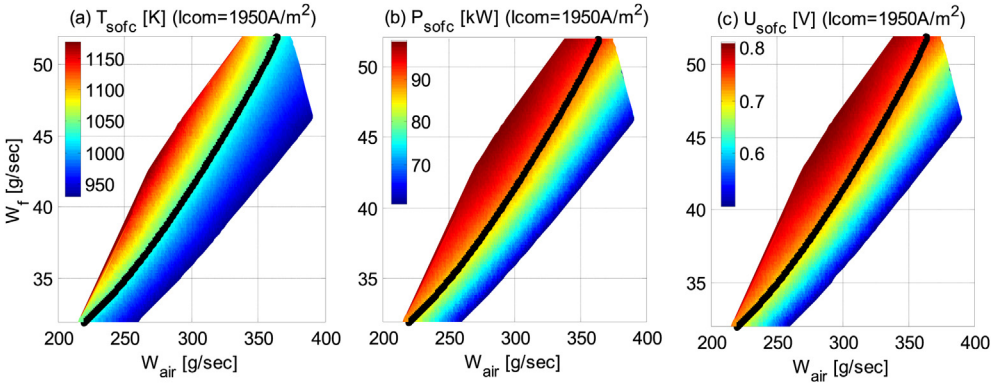


**Fig. 8.** SOFC performance with fixed current input (along the solid line, SOFC temperature is constant at 1040 K).

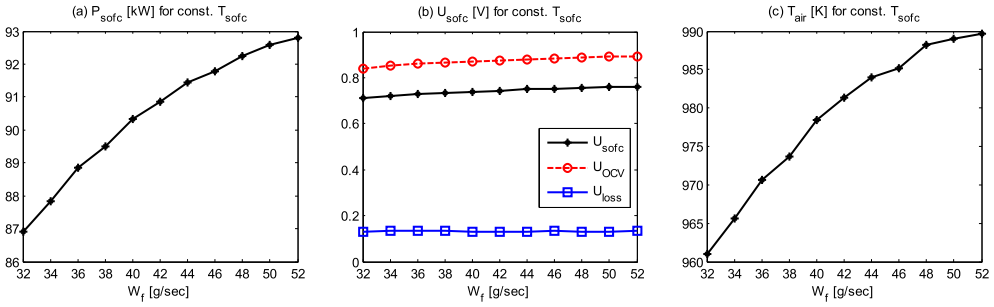


**Fig. 9.** Operating variables for constant SOFC temperature operation.

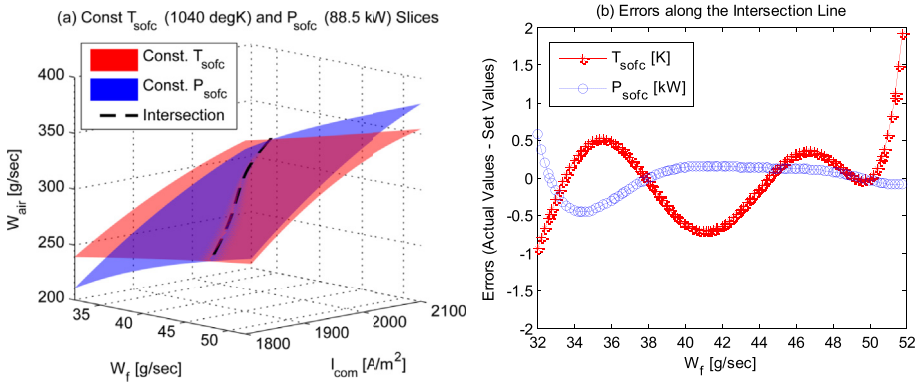


**Fig. 10.** Maintain fairly constant SOFC power and temperature.

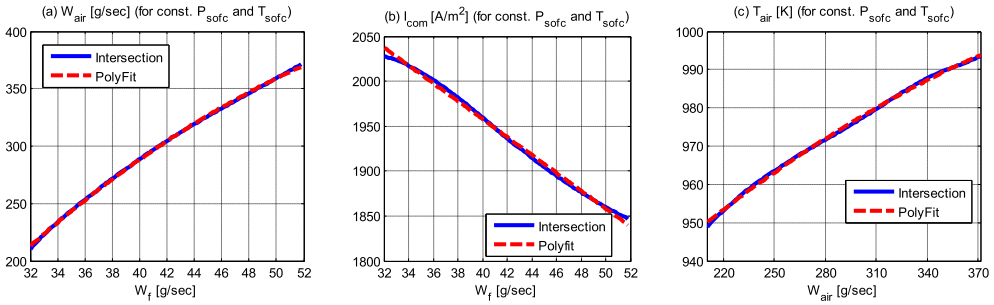


**Fig. 11.** Strategies to maintain fairly constant SOFC power and temperature: (a) air flow $W_{air}$; (b) SOFC current density $I_{com}$; and (c) SOFC inlet air temperature $T_{air}$.

$$T_{air} = f_{Tair}(W_{air}) = k_{Tair2}(W_{air})^2 + k_{Tair1}W_{air} + k_{Tair0}, \quad (12)$$

$$I_{com} = f_{Icom}\left(W_f\right) = k_{Icom1}W_f + k_{Icom0}. \quad (13)$$

Based on the above analysis, an effective SOFC operation strategy, which can be used to coordinate the SOFC inputs to keep fairly constant $T_{sofc}$ and $P_{sofc}$, is proposed as follows:

- First, determine the air-fuel ratio: analogous to power sources such as the internal combustion engines, a linear relation between the air and fuel flows is expected for the proposed S-SOFC/GT system. However, it is observed that a quadratic relationship (quite close to linear, see Fig. 11 (a) for the plot) between the inlet air flow $W_{air}$ and fuel flow $W_f$, as defined in (11), gives better results in this study.
- Second, determine the inlet air flow and temperature relation: to keep fairly constant cell temperature, the SOFC inlet air temperature $T_{air}$ should be increased to counteract the cooling effect when more air is delivered to the SOFC, as shown in Fig. 11 (c). To this end, a quadratic relation between $W_{air}$ and $T_{air}$, as defined in (12), is used for the proposed S-SOFC/GT system.
- Third, find a relation between the current density and fuel flow: by using (11) and (12), both $W_{air}$ and $T_{air}$ can be expressed as functions of $W_f$. In this case, there are two independent input variables left for the SOFC block, i.e., $W_f$ and $I_{com}$. An appropriate relation between these two variables, which can be used to limit the variations of $T_{sofc}$ and $P_{sofc}$ over the entire load range, can be determined through model-based (steady-state) simulations, as shown in Fig. 11 (b). In particular, a linear relation, as defined in (13), is able to achieve the objective.

### 3.2. A design procedure for the sprinter-SOFC/GT systems

As shown in Fig. 12, a design procedure, which helps to determine the size of different components and the reference steady-state operation line, is formulated for the proposed S-SOFC/GT system as follows:

- **Step-I**: we determine the SOFC stack parameters. Based on the cell performance data and empirical parameters (e.g., the power split ratio $P_{gen}/P_{net}$), the SOFC stack parameters (e.g., cell number $N_{cell}$, $P_{sofc}$, and $T_{sofc}$) can be determined according to the baseline power requirement. For the target system, 960 tubular cells (Section 2.2) are selected to produce an SOFC power of 88.5 kW with the cell temperature at around 1040 K.
- **Step-II**: we determine the GT parameters. To this end, the proposed SOFC operation strategy (Section 3.1), in which the SOFC inputs $W_{air}$, $T_{air}$ and $I_{com}$ are expressed as functions of $W_f$, is used to maintain fairly constant $P_{sofc}$ and $T_{sofc}$ over the entire load range. Consequently, a relation between the burner temperature $T_{cb}$ and the turbine mass flow $W_t$ (which equals the burner mass flow $W_{cb}$) can be determined from the simulation results of the SOFC and CB blocks. We can pick the initial values for the compressor pressure ratio $PR_c$ and turbine expansion ratio $ER_t$ from available GT maps (see Figs. 6 and 7 for example). In doing so, there is only one unknown variable $W_t$ (i.e., the turbine mass flow), which can determined by matching the associated shaft power $P_{gen}(W_t)$ with $P_{gen}(peak)$ to meet the peak power demand. For the target system, a slightly up-scaled (scaled up by a factor of 1.091, see Fig. 14 for the scaled map) Garrett compressor [30] (see Fig. 6 for the original map) and the radial turbine in Fig. 7 are selected.

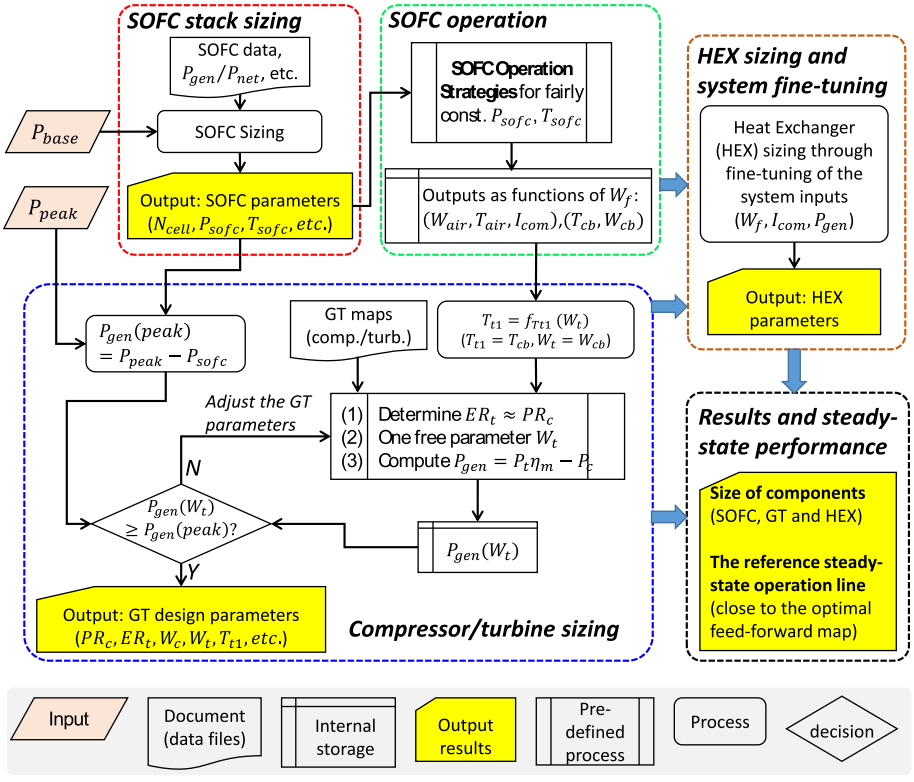


**Fig. 12.** A design procedure for the proposed S-SOFC/GT systems.

- **Step-III**: we determine the HEX parameters. It should be pointed out that in the basic system setup in which no active control of $T_{air}$ is available, small variations of the HEX coefficients are required for different loads to maintain fairly constant $T_{sofc}$ and $P_{sofc}$ over the entire load range. In this case, we can select the mean value of the calculated HEX coefficients and tune the integrated system inputs, e.g., fine-tuning $P_{gen}$ and/or $I_{com}$ for a given $W_f$, to get the desired results. In this study, the HEX is sized to have a logarithmic mean temperature difference (*LMTD*) around 120 K, thereby keep the SOFC inlet air temperature $T_{air}$ within appropriate range.

Table 2 lists key parameter values for the target system, as the result of applying the proposed design procedure. The proposed design procedure also helps to determine the reference steady-state operation line (see Fig. 14 for its location in the compressor map), which is expected to be close to the optimal feed-forward operation map.

As discussed in Section 1.2, the dynamic load following of the S-SOFC/GT system is mainly accomplished by the GT-generator, whose rotational dynamics is dominated by its effective rotational inertia, as shown in Eqn. (1), as well as the control solutions. In order to achieve fast load following operation of the S-SOFC/GT system, the GT-generator assembly consisting of low-inertia, high-speed generator/motor [39] and turbocharger [30] should be used. The solutions to the dynamic control problems will be addressed in full detail in our follow-up papers.

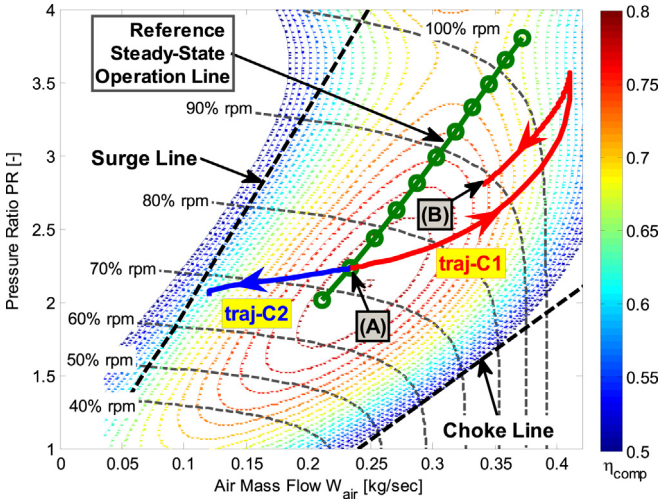


**Fig. 14.** The reference steady-state operation line and simulated trajectories plotted in the compressor map.

### 3.3. Steady-state performance of the proposed system

Fig. 13 shows the steady-state performance of the designed S-SOFC/GT system along the reference operation line. The three system inputs, i.e., the fuel flow $W_f$, the current density $I_{com}$ and the generator load $P_{gen}$, are plotted in Fig. 13 (a). Note that slight

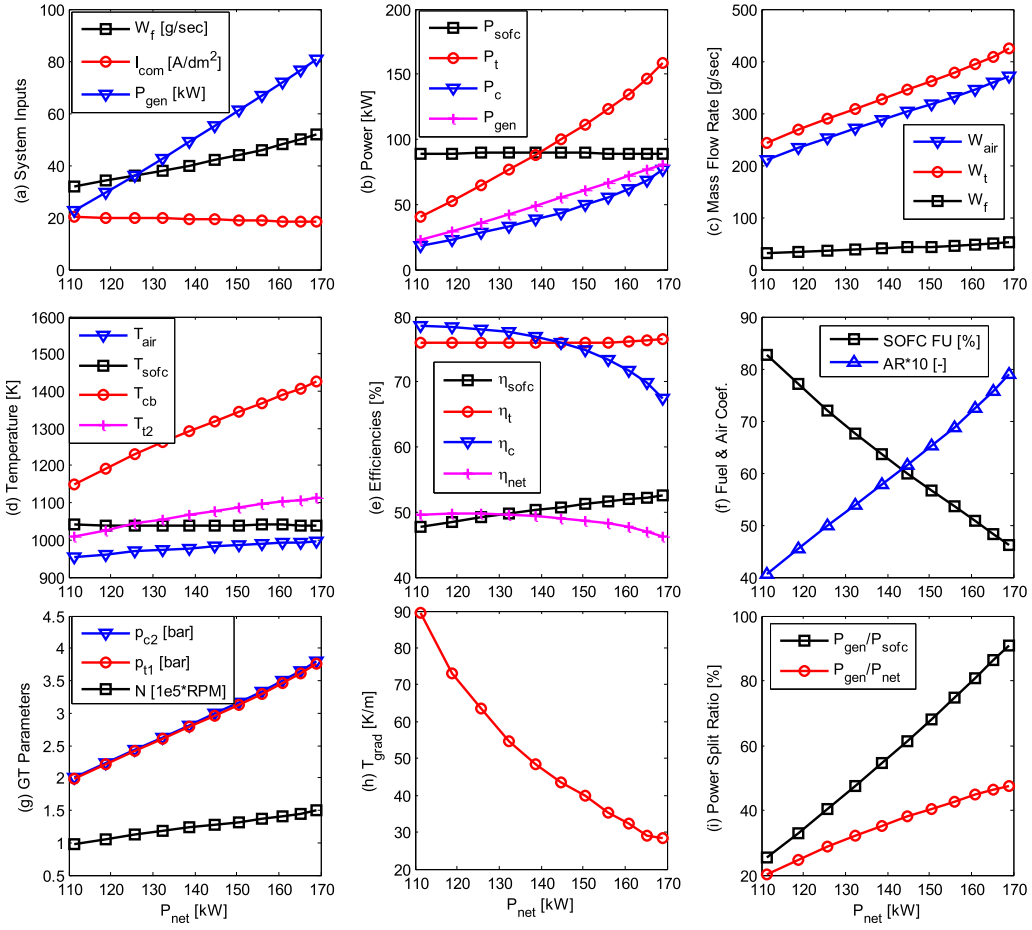


**Fig. 13.** Steady-State performance of the designed sprinter-SOFC/GT system.

**Table 2**
Key parameters for the target S-SOFC/GT system.

| Components | Key parameter values |
|---|---|
| SOFC stack | $N_{cell}$=960, $P_{sofc}$=88.5±1.0 kW, $T_{sofc}$≈1040±2 K, $W_f$=32~52 g·sec$^{-1}$, $I_{com}$=1840~2040 $A$ m$^{-2}$ |
| Compressor | $PR_c$≈3.50, $N_{cdesign}$=1.44e5 RPM, $W_{cdesign}$=360 g sec$^{-1}$ |
| Turbine | $ER_t$≈3.50, $N_{t_{design}}$ = 1.44e5 $RPM$, $T_{t1_{design}}$ = 1273$K$(1000°$C$) |
| Heat exchanger | The logarithmic mean temperature difference $LMTD$ ≈ 120 K |
| Hybrid system | $P_{base}$=110 kW, $P_{peak}$=170 kW, $\eta_{net}$=45~50% |

decrease of $I_{com}$ (with respect to $P_{net}$) is required to limit the variations of $P_{sofc}$ and $T_{sofc}$ according to the proposed operation strategy (Section 3.1). This is different from the R-SOFC/GT system, where $I_{com}$ is an increasing function of $P_{net}$ [15]. Moreover, fairly constant SOFC power and temperature have been achieved over the entire load region, as shown in Fig. 13 (b) and (d). Therefore, the proposed S-SOFC/GT system could achieve the desired steady-state performance. As shown in Fig. 13 (e), more than 45% net efficiency $\eta_{net}$ has been achieved over the entire load region. In addition, as the net power demand $P_{net}$ increases from the baseline power $P_{base}$ to peak power $P_{peak}$, the overall system efficiency $\eta_{net}$ decreases from 50% to around 46% because more power is produced by the less efficient GT-generator. Moreover, we evaluated the S-SOFC/GT system against its R-SOFC/GT counterpart in terms of fuel-to-electric efficiency along the optimal steady-state operation line [14], i.e., the static feedforward map [15]. The S-SOFC/GT system has a lower efficiency, i.e., 46.8%–50.2%, compared with the R-SOFC/GT system, which has an efficiency of 55.5%–56.1%. Therefore, fast load following operation of the S-SOFC/GT system is actually achieved by sacrificing the system efficiency.

As the net power demand $P_{net}$ increases, the GT shaft speed $N$ (Fig. 13 (g)) is increased to deliver more air $W_{air}$ (Fig. 13 (c)) to the SOFC stack while more un-reacted fuel (the SOFC fuel utilization $FU$ keeps decreasing, as shown in Fig. 13 (f)) is burnt in the burner to drive the GT-generator to produce more electric power $P_{gen}$ (see Fig. 13 (c)). The mass flow $W_t$, the inlet temperature $T_{t1}$ and inlet pressure $p_{t1}$ ($p_{t1}$=$p_{cb}$) are elevated for the turbine to produce more generator power as the load request $P_{net}$ increases, as shown in Fig. 13 (c), (d) and (g). Consequently, the power split ratios (Fig. 13 (i)) vary significantly over the entire load range. For example, the power fraction $P_{gen}/P_{sofc}$ increases from 25% to around 90%, as $P_{net}$ increases from the baseline to peak power. This is different from the conventional R-SOFC/GT system, in which the $P_{gen}/P_{sofc}$ ratio is often less than 25% [3]. In addition, unlike the R-SOFC/GT system, in which the SOFC excess air ratio $AR$ decreases with respect to $P_{net}$ [14]; the excess air ratio $AR$ is an increasing function of $P_{net}$ for the proposed S-SOFC/GT system, as shown in Fig. 13 (f). This leads to a more uniform cell temperature distribution along the SOFC, e.g., the axial direction cell temperature gradient $T_{grad}$ decreases as $P_{net}$ increases (see Fig. 13 (h)). This is another benefit (which leads to long life cycle operation) for the S-SOFC/GT system compared against the traditional R-SOFC/GT system.

It should be noted that various system operational safety factors [14] such as those related to SOFC cracking, component overheating, compressor surge and GT over-speed are considered in our research. In particular, these safety factors are used to determine the feasible operation envelope of the S-SOFC/GT system. Detailed discussions in these subjects and comparisons with the traditional R-SOFC/GT system will be presented in our follow-up papers.

## 4. Control analysis of the sprinter-SOFC/GT systems

In Section 4.1, we will investigate the control analysis for steady-state operation. The feasibility problem of fast and safe transient operation will be investigated for the proposed S-SOFC/GT system in Section 4.2.

### 4.1. Control analysis for the steady-state operation

The SOFC/GT system has three inputs: the fuel flow $W_f$, the current density $I_{com}$, and the generator load $P_{gen}$. As discussed in Refs. [14], the integrated R-SOFC/GT system is claimed to be unstable with a fixed constant $P_{gen}$ input in some regions of the feasible operation envelope. The reason is that a lower $P_{gen}$ will accelerate the shaft while a step increase of $P_{gen}$ will decelerate the shaft with no new equilibrium can be found within the valid bounds of the shaft speed [14]. Variable shaft speed control is usually used to solve this problem [4], [14]. In this section, we will demonstrate the stability problem (i.e., stability with fixed $P_{gen}$ input) through numerical case studies and develop appropriate control strategy for the proposed S-SOFC/GT system. Detailed (theoretical) analysis regarding stability of the steady-state operation will be pursued in the future.

Without loss of generality, the steady-state operation point for $P_{net}$=118.7 kW ($W_f$=34 g·s$^{-1}$) is selected in the following analysis. The point (A) in Fig. 14 corresponds to the selected steady-state operation point. We assume that the system works at the steady-state operation point (A) initially. Fig. 15 presents the simulation results of the following case studies while Fig. 14 presents the corresponding trajectories on the compressor map.

**Case-C1**: a small (<0.1%) step decrease of $P_{gen}$ is applied to the system. An abrupt increase of the shaft speed can be observed due to the rapid increase of net GT shaft power $\Delta P$ ($\Delta P$=$P_{tc}$–$P_{gen}$), as shown in Fig. 15 (a) and (d). Consequently, a significant amount of air is delivered to cool the SOFC stack rapidly, thereby leading to extremely low SOFC power generation, as shown in Fig. 15 (e) and (f). Note that the system will eventually settle at the point (B) (see Fig. 14, located at the high flow region in the compressor map). However, both $T_{sofc}$ and $P_{sofc}$ are far away from their desired values, as shown in Case-C1 of Fig. 15.

**Case-C2**: a small (<0.1%) step increase of $P_{gen}$ is applied to the system. The shaft decelerates rapidly because there is not enough shaft power to meet the $P_{gen}$ demand, as shown in Fig. 15 (a) and (d). Further drop of net shaft power $\Delta P$ due to the reduced shaft speed will lead to an irreversible process, which will cause the dangerous compressor surge [14] and system shutdown. Therefore, the integrated SOFC/GT system tends to be unstable with a fixed $P_{gen}$ input at operation point (A).

**Case-C3**: GT shaft speed control is used to stabilize the system. Feedback control of the air flow [14] or shaft speed is often used to stabilize the SOFC/GT system. In this paper, a PI-type shaft speed controller, as expressed in (14), is implemented to stabilize the S-SOFC/GT system (see Case-C3 in Fig. 15):

$$P_{gen}(s) = (k_P + k_I/s)\big(N(s) - N_{des}(s)\big), \tag{14}$$

where $N_{des}$ is the desired steady-state shaft speed corresponding to the selected operation point with a net power demand $P_{des}$. The relation between the desired shaft speed $N_{des}$ and the net power demand $P_{des}$ can be determined from the reference steady-state operation line (see Fig. 13). In this case study, a step-up (<0.1% $P_{gen}$) and a step-down (<0.1% $P_{gen}$) shaft power perturbation are applied to GT (to emulate varying resistance torque) at 100-sec and 1000-sec, respectively. As shown in Fig. 15 (Case-C3), the proposed

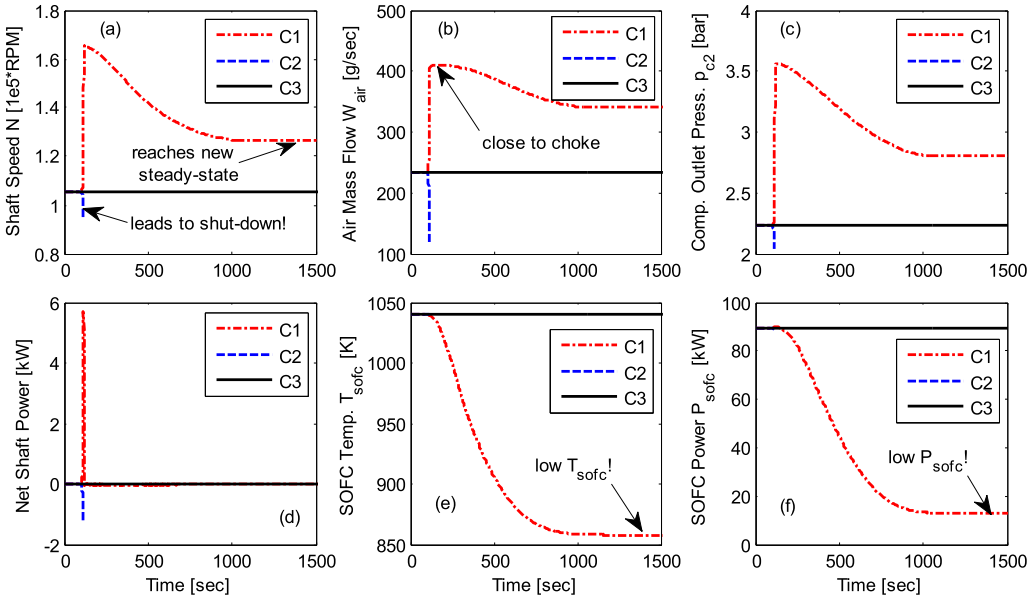


**Fig. 15.** Simulation results for steady-state operations of the S-SOFC/GT system. A small (<0.1%) step decrease of $P_{gen}$ and a small (<0.1%) step increase of $P_{gen}$ are applied to the system in Case-C1 and Case-C2, respectively. For Case-C3, a PI-type shaft speed stabilizes the system when shaft power perturbation is applied.

shaft speed controller (with $k_P$=5W/RPM, $k_P$=10W/RPM) is able to stabilize the system at desired operation point.

Similar analysis has been performed for other operation points along the reference steady-state operation line (see Fig. 14). The simulation results indicate that the (steady-state) operation points for the proposed S-SOFC/GT system tend to be unstable, especially for those located at the low and medium air flow region. Detailed (theoretical) analysis regarding stability of the steady-state operation will be pursued in the future.

### 4.2. Feasibility study for transient operations

In this section, we investigate the load following feasibility problem, i.e., whether the proposed S-SOFC/GT system could achieve fast and safe transient operations. To this end, we propose a simple control strategy by extending the shaft speed control in (14) to transient operations. From the steady-state operation map (see Fig. 13), we can find a one-to-one relation between the steady-state vector $(W_f, I_{com}, P_{gen}, N)^{ss}$ and the net power $P^{ss}_{net}$. Then, we can create the following look-up table (LUT) functions:

$$N^{ss} = N_{LUT}\left(W_f^{ss}\right), \quad I^{ss}_{com} = I_{LUT}\left(W_f^{ss}\right), \quad P^{ss}_{gen} = P_{LUT}\left(W_f^{ss}\right). \tag{15}$$

Consider a load step-up transition from $P^{ss}_{net}(S) = 110kW$ to $P^{ss}_{net}(T) = 170kW$ (i.e., step-up transition from the baseline power to peak power demand) for example. Taking the fuel path dynamics into consideration, the fuel flow $W_f$ is assumed to ramp from $W_f^{ss}(P^{ss}_{net}(S))$ to $W_f^{ss}(P^{ss}_{net}(T))$ in a time $t_r$ period. We assume that the current density $I_{com}$ is controlled by following the LUT function $I_{com}=I_{LUT}(W_f)$ in (15) for constant $P_{sofc}$ generation. In this case, if $P_{gen}$ is commanded according to the LUT function $P_{LUT}(W_f)$ directly for fast load following, the system will shutdown due to abruptly decreasing shaft speed. The reason is that there is not enough GT power to meet the fast increasing $P_{gen}$ demand. To solve this problem, the following control approach is developed for the load step-up transition by using the shaft speed controller in (14) with the desired speed equals $N_{LUT}(W_f)$:

$$\textbf{\textit{Controller I}}: \quad P_{gen}(s) = P_{LUT}\left(W_f(s)\right) + (k_P + k_I/s)\left(N(s) - N_{LUT}\left(W_f(s)\right)\right). \tag{16}$$

Simulation results of four cases with $t_r$ (i.e., ramping time of fuel flow) from 2.5 to 10.0 s are presented in Figs. 16 and 17. As shown in Fig. 16 (a), fast power transients have been achieved for all cases with power settling time less than 15 s. The generator power $P_{gen}$ is reduced to rapidly accelerate the shaft to the desired speed $N_{des}$, as shown in Fig. 16 (b) and (c). As the shaft speed increases, a significant amount of air (Fig. 16 (d)) is delivered to the burner to react with the unused fuel from the SOFC exhaust ($FU$<0.50 at peak power). Consequently, a significant amount of shaft power can be produced by the turbine to drive the generator to meet the net power demand. Moreover, the cell temperature $T_{sofc}$ remains fairly constant ($T_{sofc}$=1040±2.5 K) while the cell temperature change rate (with an absolute value less than 7 K/min) remains in an acceptable range [7], as shown in Fig. 17 (a) and (b), respectively. Note that $T_{sofc}$ first decreases due to the cooling effect of fast increasing air flow and then slowly reaches the desired steady-state value. The maximum absolute values for the cell temperature change rates decrease as $t_r$ decreases, as shown in Fig. 17 (a). Meanwhile, the SOFC power $P_{sofc}$ remains fairly constant ($P_{sofc}$=89±1.5 kW) during transients. Table 3 summarizes the controller performance.

The anode–cathode differential pressure [41,42], which is critical to SOFC safety, is also kept in a safe range (e.g., less than 30 mbar) during transient operations. Note that the anodic recirculation is not included in the current model in order to simplify the analysis and focus on the couplings of SOFC and GT [34]. As discussed in Refs. [42], the anode–cathode differential pressure depends on the anodic flow rate. Therefore, great care must be taken, especially for the anodic recirculation loop, when developing control algorithms for practical applications.

It should be noted that Controller-I in (16) has some limitations. First, the control strategy leads to considerable transient power tracking error during transients, as shown in Fig. 17 (c). Note that the normalized power tracking error is defined as

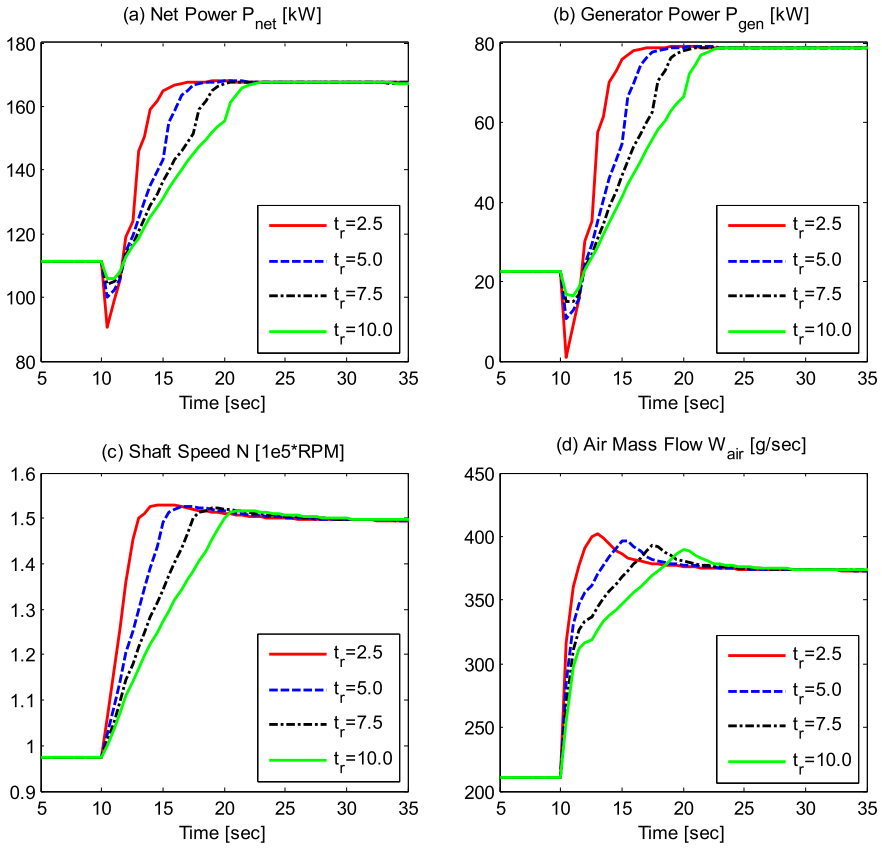


**Fig. 16.** Simulation results for load step-up transient operations (Controller-I).

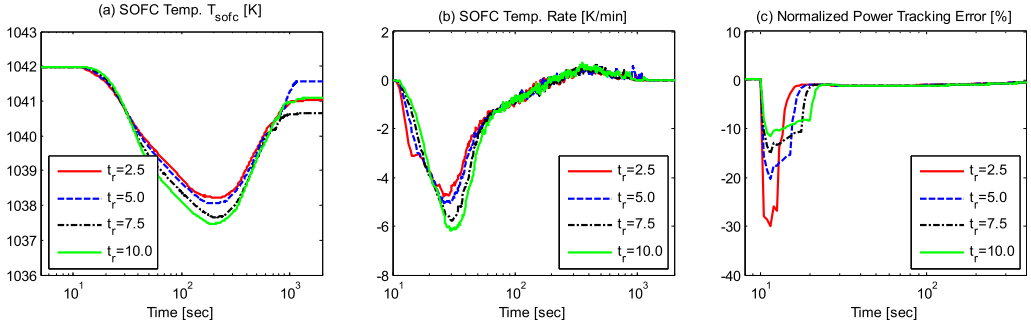


**Fig. 17.** Load step-up transient results for Controller-I (logarithmic time scale).

$\Delta P_{net}^{norm} = 1 - P_{net}/P_{net}^{ss}(W_f)$. Most of the deficit power is used to accelerate the shaft speed; therefore, it is stored in the form of mechanical energy. In this case, energy storage (battery) can be used to provide the bridging power [7]. Second, the controller may lead to over-aggressive adjustment of the air flow (Fig. 16 (d)), which might cause SOFC degradation due to thermally induced stresses. An SOFC bypass valve can be used to mitigate this problem [3]. In this paper, to reduce the cell temperature variations, a first-order transfer function, as shown in (17), is applied to the desired shaft speed $N_{des}$ which dominates the air flow.

$$\textbf{\textit{Controller II}}:\ P_{gen}(s) = P_{LUT}\left(W_f(s)\right) + \left(k_P + \frac{k_I}{s}\right)\left(N(s) - \frac{1}{\tau_N s + 1} N_{LUT}\left(W_f(s)\right)\right) \quad (17)$$

The simulation results with Controller-II in (17) with time constant $\tau_N$=4 *s* are presented in Figs. 18 and 19. As shown in Fig. 18 (a) and (b), smoother profiles for $P_{net}$ and $P_{gen}$ (note that smooth $P_{gen}$ profile is easy to implement on the hardware) have been attained by the updated controller (17) at the expense of increased power settling time (see Table 3). The updated controller (17) also reduces the SOFC power ($P_{sofc}$=89±1.0 kW) and temperature variations ($T_{sofc}$=1040±2.0 K) during transients, as shown in Table 3. Moreover, compared to Controller-I (see Fig. 16 (d)), the updated controller (17) smoothes the of air flow variations (see Fig. 18 (c)), thereby leading to smaller cell temperature change rates (with absolute values less than 4 K·min$^{-1}$) for safer SOFC operations, as shown in Fig. 19 (b). Therefore, the proposed S-SOFC/GT system holds the promise to achieve the desired performance with fairly constant SOFC temperature and power, and acceptable $T_{sofc}$ changing rate for safe transient operations. The simulation results

**Table 3**
Summary of the controller performances.

| Controller | Controller-I | | | | Controller-II | | | |
|---|---|---|---|---|---|---|---|---|
| Fuel ramping time $t_r$ [sec] | 2.5 | 5.0 | 7.5 | 10.0 | 2.5 | 5.0 | 7.5 | 10.0 |
| Settling time (2% $P_{net}$ error) [sec] | 6.0 | 7.5 | 10.0 | 12.0 | 12.0 | 13.5 | 15.0 | 17.0 |
| Max $T_{sofc}$ variations [K] | 1.77 | 1.95 | 2.33 | 2.50 | 1.24 | 1.28 | 1.31 | 1.43 |
| Max $T_{sofc}$ changing rates [K/min] | 4.73 | 5.06 | 5.78 | 6.20 | 3.08 | 3.37 | 3.72 | 3.87 |
| Max $P_{sofc}$ variations [kW] | 0.88 | 1.08 | 1.18 | 1.23 | 0.68 | 0.80 | 9.82 | 0.91 |

also indicate that the proposed S-SOFC/GT system has far improved transient capabilities than the traditional R-SOFC/GT systems.

It should be noted that the lack of independent air control poses a serious challenge for the transient operations for the S-SOFC/GT system since both load following and the air flow management are dictated by the generator power $P_{gen}$ [14] in the basic system setup. For example, fast step-up load transient requires fast increasing generator power (note that the SOFC power $P_{sofc}$ remains fairly constant during the transient). However, the rapid increase of $P_{gen}$ might reduce the shaft speed and affect the CB air flow supply, thereby limiting the turbine power generation capability to meet the desired power demand. Therefore, better trade-off between fast load following and air flow management should be obtained for improved transient performance. It should be noted that there are also some other transient operation problems. For example, as pointed out in Refs. [38], large steps of load reduction often induce less controllable compressor operation, which might cause the dangerous compressor surge [14]. To this end, control algorithms (e.g., MPC) will be pursed for coordinated power and thermal management in the future.

## 5. Summary and future work

To meet fast and safe load following requirements for mobile applications, a sprinter-SOFC/GT system concept, in which a constant loading SOFC provides the baseline power while the GT-generator is used for fast dynamic load following, is proposed in this paper. System design and control studies have been conducted by using an SOFC/GT system model consisting of experimentally-verified component models. In particular, an SOFC operation strategy is proposed to keep fairly constant SOFC power and temperature (steady-state values) over the entire load range. A system design procedure has been proposed to determine the size of different components and the reference steady-state operation line. In addition, control analysis has been investigated for both steady-state and transient operations. The feasibility study simulation results suggest that the proposed S-SOFC/GT system holds the promise to achieve fast and safe load following by taking full advantage of the GT-generator fast dynamic capability while keeping fairly constant SOFC power and temperature. Although the results presented in this paper are specific for a specific target power system, i.e., the primary electric propulsion system for military ground vehicles, the proposed design procedure and analysis methodology are more general, and can be applied to other size power systems.

In the future, we will identify the feasible operation regimes of the proposed S-SOFC/GT system by considering various safety factors such as those related to SOFC cracking and component overheating. System optimization and further transient control strategies will also be investigated. In addition, the S-SOFC/GT

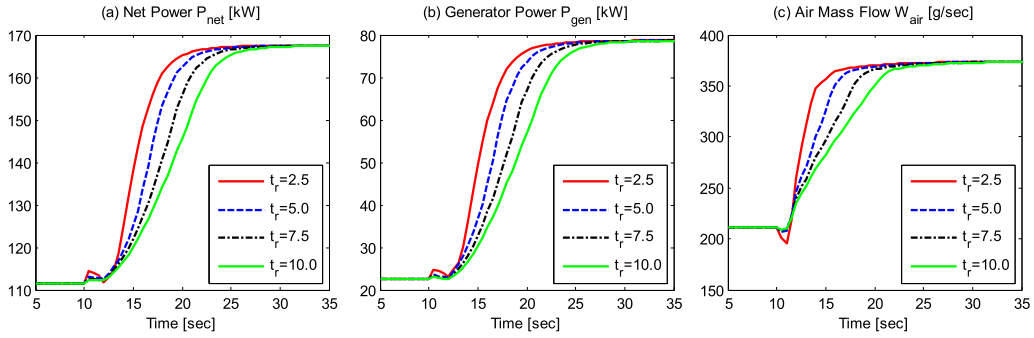


**Fig. 18.** Simulation results for load step-up transient operations (Controller-II).

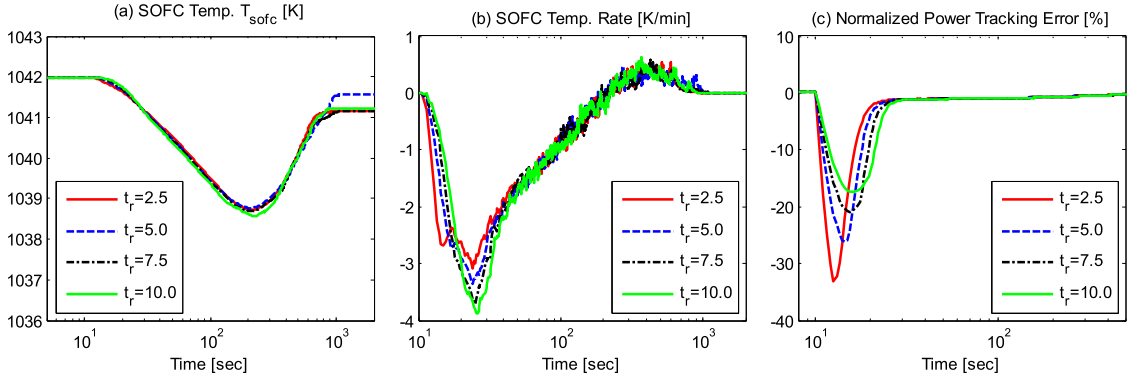


**Fig. 19.** Load step-up transient results for Controller-II (logarithmic time scale).

system will be studied with respect to the conventional R-SOFC/GT system in terms of the feasible operation regime, steady-state and transient performance. The future work also includes the study of variant system configurations, e.g., the basic system setup augmented with additional components such as energy storage and bypass valves [4].

## Acknowledgment

The authors would like to acknowledge the Automotive Research Center (US Army TARDEC) for the support of this research.

## References

[1] Subhash Singhal, High-temperature Solid Oxide Fuel Cells: Fundamentals, Design and Applications: Fundamentals, Design and Applications, Elsevier, 2003.
[2] James Larminie, Andrew Dicks, Maurice S. McDonald, Fuel Cell Systems Explained, Vol. 2, Wiley, Chichester, 2003.
[3] J. Brouwer, Hybrid gas turbine fuel cell systems, Chapter 4, in: Richard A. Dennis (Ed.), The Gas Turbine Handbook, U.S. Department of Energy, Morgantown, West Virginia, 2006. DOE/NETL-2006/1230.
[4] J. Brouwer, Fuel Cell & Hybrid Fuel Cell Gas Turbine System Design, Dynamics & Control, National Fuel Cell Research Center (NFCRC) presentation slides, April 18, 2011.
[5] Farshid Zabihian, Alan Fung, A review on modeling of hybrid solid oxide fuel cell systems, Int. J. Eng. 3 (2) (2009) 85–119.
[6] So-Ryeok Oh, Jing Sun, Optimization and load-following characteristics of 5kw-class tubular solid oxide fuel cell/gas turbine hybrid systems, in: American Control Conference (ACC), 2010, IEEE, 2010.
[7] Zhenzhong Jia, Jing Sun, So-Ryeok Oh, Herb Dobbs, Joel King, Control of the dual mode operation of generator/motor in SOFC/GT-based APU for extended dynamic capabilities, J. Power Sources 235 (2013) 172–180.
[8] Christopher J. Steffen Jr., Joshua E. Freeh, Louis M. Larosiliere, Solid oxide fuel cell/gas turbine hybrid cycle technology for auxiliary aerospace power, in: ASME Turbo Expo. Reno-Tahoe, United States, 2005.
[9] Wolfgang Winkler, Hagen Lorenz, The design of stationary and mobile solid oxide fuel cell–gas turbine systems, J. Power Sources 105 (2) (2002) 222–227.
[10] Ruixian Fant, et al., System-level thermal modeling and co-simulation with hybrid power system for future all electric ship, in: Electric Ship Technologies Symposium, 2009. ESTS 2009, IEEE, 2009.
[11] Jing Sun, John Stebe, Colen Kennell, Feasibility and design implications of fuel cell power for sealift ships, Nav. Eng. J. 122 (3) (2010) 87–102.
[12] So-Ryeok Oh, Jing Sun, Herb Dobbs, Joel King, Model-based predictive control strategy for a solid oxide fuel cell system integrated with a turbocharger, in: American Control Conference (ACC), 2012, pp. 6596–6601.
[13] Christoph Stiller, Bjørn Thorud, Olav Bolland, Rambabu Kandepu, Lars Imsland, Control strategy for a solid oxide fuel cell and gas turbine hybrid system, J. power sources 158 (1) (2006) 303–315.
[14] Christoph Stiller, Design, Operation and Control Modelling of SOFC/GT Hybrid Systems (PhD thesis), Department of Energy and Process Engineering, Norwegian University of Science and Technology, Trondheim, Norway, March 2006.
[15] Vasilis Tsourapas, Control Analysis of Integrated Fuel Cell Systems with Energy Recuperation Devices (PhD thesis), University of Michigan, Ann Arbor, MI, USA, 2007.
[16] Caihao Weng, Jing Sun, Design of a variable geometry turbine control strategy for solid oxide fuel cell and gas turbine hybrid systems, in: American Control Conference (ACC), 2012, IEEE, 2012.
[17] G. Sieros, K.D. Papailiou, Gas turbine components optimised for use in hybrid SOFC-GT systems, in: Proceedings of 7th European Conference on Turbomachinery Fluid Dynamics and Thermodynamics, Athens, Greece, 2007.
[18] F. Calise, A. Palombo, L. Vanoli, Design and partial load exergy analysis of hybrid SOFC–GT power plant, J. power sources 158 (1) (2006) 225–244.
[19] J. Palsson, Azra Selimovic, Design and Off-design Predictions of a Combined SOFC and Gas Turbine System, ASME paper 2001-GT-0379, 2001.
[20] David Tucker, Larry Lawson, Thomas P. . Smith, Comas Haynes, Evaluation of cathodic air flow transients in a hybrid system using hardware simulation, in: The 4th International Conference on Fuel Cell Science, Engineering and Technology, Irvine, CA, June 19-21, 2006.
[21] P. Costamagna, L. Magistri, A.F. Massardo, Design and part-load performance of a hybrid system based on a solid oxide fuel cell reactor and a micro gas turbine, J. Power Sources 96 (2) (2001) 352–368.
[22] S.H. Chan, H.K. Ho, Y. Tian, Modelling for part-load operation of solid oxide fuel cell–gas turbine hybrid power plant, J. Power Sources 114 (2) (2003) 213–227.
[23] David Hall, Transient Modeling and Simulation of a Solid Oxide Fuel Cell (PhD thesis), University of Pittsburgh, 1997.
[24] Handa Xi, Dynamic Modeling and Control of Planar SOFC Power Systems (PhD thesis), University of Michigan, Ann Arbor, MI, USA, 2007.
[25] Erian A. Baskharone, Principles of Turbomachinery in Air-Breathing Engines, Cambridge University Press, 2006.
[26] F. Payri, J.R. Serrano, P. Fajardo, M.A. Reyes-Belmonte, R. Gozalbo-Belles, A physically based methodology to extrapolate performance maps of radial turbines, Energy Convers. Manag. 55 (2012) 149–163.
[27] N. Karamanis, R.F. Martinez-Botas, Mixed-flow turbines for automotive turbochargers: steady and unsteady performance, Int. J. Engine Res. 3 (3) (2002) 127–138.
[28] Paul Moraal, Ilya Kolmanovsky, Turbocharger modeling for automotive control applications, SAE Trans. 108 (3) (1999) 1324–1338.
[29] Torkel Glad, Andey Sokolov, Identifiability of Turbocharged IC Engine Models, in: Proceedings of the SAE 1999 International Congress & Exposition, 1999.
[30] Garrett Turbochargers. http://www.turbobygarrett.com.
[31] Stephen E. Veyo, et al., Tubular solid oxide fuel cell/gas turbine hybrid cycle power systems: status, J. Eng. Gas Turbines Power 124 (4) (2002) 845–849.
[32] http://www.mhi.co.jp/en/technology/business/power/sofc/development_situation.html(Mitsubishi Heavy Industries, Ltd, Japan).
[33] Debangsu Bhattacharyya, Raghunathan Rengaswamy, A review of solid oxide fuel cell (SOFC) dynamic models, Industrial Eng. Chem. Res. 48 (13) (2009) 6068–6086.
[34] S.-R. Oh, Jing Sun, Herb Dobbs, Joel King, Performance evaluation of solid oxide fuel cell engines integrated with single/dual-spool turbochargers, J. Fuel Cell Sci. Technol. 8 (6) (2011).
[35] Alberto Traverso, et al., Gas turbine assessment for air management of pressurized SOFC/GT hybrid systems, J. Fuel Cell Sci. Technol. 4 (4) (2007) 373–383.
[36] A. Traverso, L. Magistri, A.F. Massardo, Turbomachinery for the air management and energy recovery in fuel cell gas turbine hybrid systems, Energy 35 (2) (2010) 764–777.
[37] http://web.mit.edu/16.unified/www/FALL/thermodynamics/notes/node131.html Thermodynamics Lecture Notes, Section 18.5: Heat Exchangers.
[38] Andre Hildebrandt, Mohsen Assadi, Sensitivity Analysis of Transient Compressor Operation Behaviour in SOFC-gt Hybrid Systems, ASME Turbo Expo 2005: Power for Land, Sea, and Air, American Society of Mechanical Engineers, 2005.
[39] Seok-Myeong Jang, Han-Wook Cho, Sang-Kyu Choi, Design and analysis of a high-speed brushless DC motor for centrifugal compressor, Magnetics, IEEE Trans. 43 (6) (2007) 2573–2575.
[40] Stefano Campanari, Thermodynamic model and parametric analysis of a tubular SOFC module, J. Power Sources 92 (1) (2001) 26–34.
[41] Mario L. Ferrari, Solid oxide fuel cell hybrid system: control strategy for stand-alone configurations, J. Power Sources 196 (5) (2011) 2682–2690.
[42] Mario L. Ferrari, Aristide F. Massardo, Cathode–anode side interaction in SOFC hybrid systems, Appl. Energy 105 (2013) 369–379.